Experimental Investigation on Cavity Pressure inside Sheet Cavitation

Kobayashi, Keisuke
Graduate School of Engineering, Kyushu University

Katayama, Yusuke
Department of Mechanical Engineering, Faculty of Engineering, Kyushu University

Watanabe, Satoshi
Department of Mechanical Engineering, Faculty of Engineering, Kyushu University

Tsuda, Shin-ichi
Department of Mechanical Engineering, Faculty of Engineering, Kyushu University

出版情報：Journal of Fluids Engineering. 143 (12), pp.121102-, 2021-12. American Society of Mechanical Engineers (ASME)
バージョン：

Experimental Investigation on Cavity Pressure inside Sheet Cavitation

Kobayashi, Keisuke
Graduate School of Engineering, Kyushu University
744 Motooka, Nishi-ku, Fukuoka 819-0395, Japan

Katayama, Yusuke
Department of Mechanical Engineering, Faculty of Engineering, Kyushu University
744 Motooka, Nishi-ku, Fukuoka 819-0395, Japan
katayama@mech.kyushu-u.ac.jp

Watanabe, Satoshi[1]
Department of Mechanical Engineering, Faculty of Engineering, Kyushu University
744 Motooka, Nishi-ku, Fukuoka 819-0395, Japan
fmnabe@mech.kyushu-u.ac.jp
ASME Membership: #000004595914

Shin-ichi Tsuda
Department of Mechanical Engineering, Faculty of Engineering, Kyushu University
744 Motooka, Nishi-ku, Fukuoka 819-0395, Japan
tsudashin@mech.kyushu-u.ac.jp

ABSTRACT

The gas content is one of the important factors in cavitation, which may increase the pressure inside the cavity through the diffusive mass transfer of the dissolved gas into the cavity. In the present study, we try to directly measure the cavity pressure inside the sheet cavity at the throat of a converging-diverging nozzle. Then the influences of the flow velocity and the gas content (amount of dissolved oxygen) on the gas partial pressure are investigated. It is found that, even in low gas content level, the cavity pressure is slightly but apparently higher than the saturated vapor pressure, indicating the presence of gas partial pressure. It is observed that the gas partial pressure in significantly developed cavitation is almost constant regardless of the flow velocity but slightly increases against the increase of the saturation level of dissolved gas. It is also found that the gas partial pressure inside cavity depends on the degree of cavitation development; the gas partial pressure decreases with the development of cavitation.

INTRODUCTION

Hydrodynamic cavitation is generally discussed by using the following cavitation number σ defined under the assumption that the pressure inside cavitation bubbles is equal to the saturated vapor pressure P_v[1].

$$\sigma = \frac{P_{ref} - P_v}{\rho V_{ref}^2/2} \tag{1}$$

where P_{ref} and V_{ref} are the reference absolute pressure and flow velocity, and ρ is the density of working fluid in liquid state. The law of similitude for cavitation using this cavitation number is often valid for the high speed flows, from which it is derived that the working pressure condition is to be proportional to the square of reference flow velocity to obtain the flow similarity. However, it is known that this similitude does not hold in some cases, which is believed to be partly or mainly due to the quality of working liquid; bubble nuclei distribution, dissolved gas content, other impurities and so forth in the case of water. Actually, an international standard ISO5198:1987 [2], which describes the code for hydraulic performance tests of pumps, mentions that the conversion of net positive suction head (NPSH) can be made using Eq. (1) under the flow similarity as a first approximation, but it may deviate due to the influences of several factors such as thermodynamic effects, the variation of the surface tension or the differences in dissolved or occluded air content. In water at room temperature, the thermodynamic effect is generally neglected because of small density ratio of the vapor and liquid phases as well-known [3], but the pressure inside the cavity still seems not to be equal to the saturated vapor pressure due to the inclusion of other gas species, air (nitrogen and oxygen).

There are a large number of studies on the effects of dissolved gas on single bubble and also on acoustic cavitation like those in ultrasonic cleaning, but the dissolved gas effects on hydrodynamic cavitation have not been well studied. In hydrodynamic cavitation studies, most of them have been devoted mainly to the cavitation inception and desinence. We have also studied the inception process of sheet cavitation along the wall of a two-dimensional convergent-divergent nozzle under the different amount of dissolved oxygen [4]. Amini et al. [5] studied the hysteresis of tip vortex cavitation around an elliptical hydrofoil and discussed the reason for the hysteresis between inception and desinence on the basis of mass diffusion of dissolved oxygen on the surface of leading edge sheet cavitation connecting to the tip vortex cavitation. The mass diffusion of dissolved gas into the cavity has been studied for natural and ventilated cavitation. Brennen [6] conducted a simplified theoretical analysis involving the turbulent boundary layers on natural supercavitation past a spherical headform to estimate the mass diffusion rate into the cavity. Billet and Weir [7] extended the Brennen's model to an axisymmetric ventilated cavity around zero-caliber ogive, and they showed the necessity of some calibration of the model. Parkin and Ravindra [8] considered Launder-Spaulding type turbulence diffusivity for more generalized analysis of convective gaseous diffusion into the cavity. More recently, Yu and Ceccio [9] measured bubble populations downstream of a stable partial cavity. Assuming that those bubbles consist of diffused gas at cavity interface, they estimated the gas flux into the sheet cavity and compare it with the models proposed in the past literature. Lee et al. [10] estimated the mass transfer coefficient of dissolved gas across the surface of sheet cavity in a convergent-divergent nozzle from the void fraction measured upstream and downstream of the nozzle by using X-ray visualization. Since such bubble releases

would give a significant impact on the performance and reliability of hydraulic systems, cavitation-induced air release in oil flow has been also a major concern among the researchers. Iben et al. [11] conducted the optical measurements of gas bubbles in cavitating oil flow behind a micro orifice, and Kowalski et al. [12] experimentally investigated the relation between cavitation intensity, that is an observed area of cavitating region, and air release in an orifice flow to understand cavitation-induced rapid degassing. Zhou et al. [13] proposed a prediction method of dynamic feature of air release and absorption in hydraulic oils in a closed system based on a simplified air release/absorption model combined with Singhal's full cavitation model [14]. Freudigmann et al. [15] also proposed a model describing cavitation-induced air release on the basis of the idea that the diffusive mass transfer of air into generated vapor cavities is a dominant mechanism of rapid degassing. However, it has not yet been well understood how much the internal pressure of cavity is affected by the dissolved gas in the liquid.

Returning the scaling law of cavitation, one may expect that the flow similitude would well hold by referring the pressure on the outer wall of cavity P_w instead of the vapor pressure for the cavitation number as below;

$$\sigma' = \frac{P_{ref} - P_w}{\rho V_{ref}^2/2}$$

From the force balance on the cavity interface, P_w can be approximated by the following Laplace's equation with neglecting the viscous shear stress:

$$P_w \cong P_v + P_g - \frac{2T}{R}$$

where P_g is a partial pressure of gas inside the cavity, T is the surface tension and R is the curvature radius of cavity interface. Therefore, the cavitation number σ can be re-written as;

$$\sigma \cong \sigma' + \psi_g - \frac{4}{We} \tag{2}$$

where $\psi_g = 2P_g/\rho V_{ref}^2$ is the normalized partial pressure of gas inside the cavity and $We = \rho V_{ref}^2 R/T$ is the Weber number. If we consider the film-like sheet cavity developed on the solid wall, the surface tension term, the third term of RHS of Eq. (2) may be negligible due to large curvature radius of sheet cavity interface. The effect of gas partial pressure, the second term of RHS, enhances the development of cavitation, which may explain the aforementioned deviation of similarity low of cavitation performance of pumps. For improvement of more quantitative conversion of suction performance, it is necessary to quantitatively predict the partial gas pressure p_g inside the cavity.

In the past literature, Gadd and Grant [16] experimentally demonstrated that the internal pressure of super cavity in water formed behind the discs exceeds the water vapor pressure because of unavoidable presence of air dissolved in the liquid. Brennen [6] also measured the internal pressure of natural super cavity behind a spherical headform and showed that the partial pressure of gas is in the order of hundred pascals and is linearly increased with the air content dissolved in water. On the other hand, Washio [17] claims on the basis of the experiment that the pressure inside cavity at the choking condition is kept almost at the vapor pressure of water so that the influence of partial gas pressure is negligible. In the present study, we try to directly measure the pressure inside the film-like sheet cavity in water at several conditions to re-visit the internal pressure of cavity and the influence of gas content on it. As a simple flow case, the convergent-divergent nozzle flow

is employed to have a sheet cavity along the nozzle wall. The gas content is roughly adjusted to some level by referring to the dissolved oxygen (DO) content of working water measured by a DO sensor. Visual observation of cavitation along with the pressure measurement is also conducted in various flow velocity, pressure and DO conditions under constant temperature.

EXPERIMENTAL METHOD

Experimental Apparatus and Measurements

The experiments were performed in a small cavitation tunnel at Kyushu University, Japan. The tunnel had been used for our previous study [18] to measure the pressure inside the sheet cavity of thermos-sensible fluid, in which thermal effect of cavitation seemed to co-appear with the effect of mass diffusion of dissolved gas. Figure 1 shows a schematic view of our cavitation tunnel. Since the tunnel is a kind of small one, it is equipped with a heat exchanger to ensure the constant water temperature (in this study 20±0.5°C) during the experiment. It also has a tank with bubble removal filter consisting of wounded polypropylene cartridge filters with the nominal pore diameter of 1μm, by which large bubble nuclei in test water can be effectively removed as has been shown in Ref. [4]. The water flow is driven by two circulating pumps in serial, and the volumetric flow rate Q is measured by an ultrasonic flow meter (Keyence, FD-Q50A, capacity: 400L/min, accuracy: 8L/min) installed just before the test section. The flow rate is regulated by the valve downstream of the bubble removal filter. The tunnel is a closed loop one, and the system pressure can be regulated at specified value by adjusting the gas pressure at the water surface in the tank using a vacuum pump connected at the top of the tank. The gas pressure is measured by a pressure transducer (GE sensing, UNIK5000, capacity: 200kPa abs,

accuracy: 200Pa) installed also at the top of the tank, and the tank pressure P_{tank} is defined by adding a hydrostatic pressure corresponding to water surface level in the tank onto the measured pressure.

Figure 2 shows a converging-diverging nozzle used in this study. The test section of the tunnel is a rectangular one with the height of H=20.1mm and the depth of B=20.0mm. A two-dimensional converging-diverging nozzle is installed at the test section. The height of nozzle throat is h=5.5mm while the depth is 20.0mm (=B). Against the converging angle of 43° of the nozzle, the diverging angle is set to be 8.4° so that the flow reattaches smoothly after the throat to have sheet cavity along the nozzle bottom wall. In the present study, in order to measure the pressure inside the sheet cavity, we prepared four pressure taps Ch. 1, 2, 3 and 4 along the nozzle bottom wall, and they are connected to individual pressure transducers (GE sensing, UNIK5000) via pressure tubes. Ch.1 is located at the nozzle throat and Ch. 2, 3 and 4 at the diverging part. Specifications of pressure transducers will be provided later. To enhance the accuracy of the pressure measurement, we located the measurement surface of pressure transducers at the same vertical location of pressure taps and tried to avoid bubble accumulations inside pressure tubes as much as we could, but it seems that we still have in-negligible errors within at most a few hundred Pa (a few centimeters in static head). We also conducted the visual observation of cavitation by using a high-speed camera to check if the pressure taps are covered by the sheet cavity or not. Then, the partial gas pressure inside the cavity is estimated.

Since we are interested in the effect of dissolved gas in water on the pressure inside sheet cavity, the gas content should be also an important parameter. In the present study, the gas content is defined by the amount of dissolved oxygen normalized by that at the

atmospheric pressure and the water temperature of 20°C, and it is denoted by DO [%] meaning the saturation level of dissolved oxygen. The gas content is adjusted to a certain under-saturated level by operating the tunnel under low pressure for degassing. The amount of dissolved oxygen DO is measured before and after each experiment by a membrane type Galvanic cell method (DKK-TOA, DO31P, capacity: 200%, accuracy: ±2%).

Experimental Conditions

In the present study, we firstly conducted the experiment #1~#5 by continuously and slowly changing the tank pressure P_{tank} to grasp the basic characteristics of partial pressure of gas inside the cavity against DO and the nozzle throat velocity U_{th} $(= Q/Bh)$. Then we conducted some detailed measurements of pressure and sheet cavity length at a certain throat velocity in the various DO conditions (experiment #6~#9). In each experiment, the cavitation number is defined as follows, referring to the upstream tank pressure P_{tank} using the nozzle throat velocity U_{th} as a representative flow velocity.

$$\sigma_{tank} = \frac{P_{tank} - P_v}{\rho U_{th}^2/2} \tag{3}$$

Note that, considering the pressure decrease due to the flow acceleration and the pressure loss between the upstream tank and the inlet of test section, the cavitation number at the test section is smaller than σ_{tank}; the difference is roughly 0.2.

Additional information on each experimental campaign will be given below.

Experimental campaign #1~#5

To investigate the effect of gas content and flow velocity on the gas pressure inside the sheet cavity, we set five experimental conditions by changing the gas content DO [%]

and the nozzle throat velocity U_{th} as summarized in Table 1. In each condition, the experiment was conducted for three times to check the repeatability of the measurement. Since the cavitation tunnel used in this study is small, it is difficult to keep the gas content at the same level for long-time experiment especially in low velocity conditions, namely #1 and #2. To minimize the change of gas content during each experiment, we continuously decreased the tank pressure P_{tank} to observe the inception and the development of sheet cavitation and then increased it to observe the desinence of sheet cavitation. Figure 3 shows examples of time histories of given change of P_{tank}, those are for the experimental campaigns of #1-1st (U_{th}=6.3m/s), #2-1st (7.9m/s) and #3-1st (9.0m/s). Each experiment took about 9 to 5 minutes for U_{th}=9.0 to 6.3m/s, and the change in the gas content DO before and after the experiment was small as shown in Table 1. Typical pressure decreasing and increasing rates dP_{tank}/dt were $-0.4\sim-0.25$ kPa/s and 0.25~0.45kPa/s, respectively. We have also checked the influence of the changing rate of P_{tank} on the pressure measurement in the case with U_{th}=9.0m/s, and it was found that this influence was not very significant. Please note that the volumetric flow rate, i.e. the throat velocity U_{th} also slightly changes during the experiment, since the pressure loss at the test section increases especially when the sheet cavity is significantly developed.

In this experimental campaign #1~#5, pressure transducers were installed for pressure taps Ch.1~Ch.3. Specification of each pressure sensor is listed in Table 2. Sampling frequency of pressure measurements was 400Hz and the moving average for the duration of 1 second was applied to enhance the measurement accuracy with the removal of flow noises from the signals. It should be noted that a high accuracy pressure transducer

was used for Ch.3, resulting in a typical uncertainty with 95% confidence level in the measurement was 13Pa including precision and bias limits.

Experimental campaign #6~#9

To investigate the effect of gas content on the gas pressure inside the sheet cavity with various degrees of cavitation development, we set totally 16 experimental conditions by changing the gas content DO [%] in four levels and the tank pressure P_{tank} in four levels as summarized in Table 3. The main number #X (6~9) indicates the different level of DO, while the branch number 1~4 indicates the different level of tank pressure, at which we observed the different size and unsteadiness of sheet cavity.

#X-1: Steady sheet cavity

#X-2: Fluctuating sheet cavity with small amplitude

#X-3: Fluctuating long sheet cavity with large amplitude

#X-4: Stable long sheet cavity

We did not observe a well-known phenomenon of cloud cavity shedding, repetitive detachment of sheet cavity by a re-entrant jet, probably because Reynolds number in the present experiment is rather small, $\mathrm{Re} = U_{th}h/\nu = 3.5\sim5.0 \times 10^4$. This agrees with the observation by Pelz et al. [19], in which the transition process from sheet to cloud cavitation was experimentally and analytically studied in a wide Reynolds number range.

Typical examples of shadowgraph images taken by high-speed camera are shown in Fig. 4. We can see many tiny bubbles behind the sheet cavity developing along the diverging wall, and the number of tiny bubbles is remarkably larger in higher gas content

level, namely in the case of DO=70%. From these photos, we can recognize if the pressure taps of Ch. 1~Ch. 4 are covered by sheet cavity or not, which is important to estimate the partial pressure of gas inside sheet cavity.

To evaluate the sheet cavity length l_c and its unsteadiness, we conducted the image analysis of shadowgraph movies taken by a high speed camera. Frame rate and resolution of images were 1000 frame/s and 512×256 pixels, respectively. The image-to-physical lengths conversion ratio was 0.25mm/pixel. We define the cavity length l_c by the distance between the throat of the nozzle and the location of the maximum thickness of cavity as shown in Fig. 5. Since the cavity surface is generally not very smooth, we firstly average several numbers (N_{ave}) of continuous images to remove meaningless cavity length fluctuations. After some trial and error, we have determined as $N_{ave} = 10$, and an example of the averaged images is shown in Fig. 5(a). Then, the image without the occurrence of cavitation is selected as a background image and is subtracted from the locally time-averaged images as shown in Fig. 5(b). Finally, the binarization of the obtained images is conducted with some threshold value which is predetermined by trial and error through the comparisons between original and processed images, and the cavity length l_c is determined as shown in Fig. 5(c). We conducted this image analysis for totally 42,794 images in each condition, and the time-averaged cavity length and the dominant frequency of cavity length fluctuation were obtained.

In this experimental campaign #6~#9, pressure transducers were installed for the pressure taps of Ch.1~Ch.4. Specification of each pressure sensor is listed in Table 4. Pressure measurements were conducted simultaneously with the high-speed filming, and therefore the sampling frequency was 1 kHz. The time-averaged pressure for 42.764

seconds was used to evaluate the partial pressure of gas P_g inside the cavity. It should be noted that a high accuracy pressure transducer was used for Ch.4, resulting in a typical uncertainty with 95% confidence level in the measurement was 13 Pa including precision and bias limits. Also, in these experiments, we changed the direction of nozzle contraction from vertical to horizontal (direction of gravity is shown in Fig. 2 (a)) so that pressure tubes which connect the pressure taps to the pressure transducers can lie horizontally, which enables us to minimize the influence of accumulated bubble onto the measured pressure; more quantitatively reliable measurement is expected to be made. Froude number was $\mathrm{Fr} = U_{th}/\sqrt{gB} \cong 20$, and we confirmed that the global behavior of sheet cavity was basically two-dimensional; influence of gravity is negligible.

RESULTS AND DISCUSSION

First of all, the results of experimental campaign #1~#5 will be presented to show the influences of flow velocity U_{th} and DO on the partial pressure of gas inside the cavity, especially on that inside the significantly developed cavitation. After that, the pressure measurements as well as the observation of cavitation conducted in experimental campaign #6~#9 will be presented to show the relation of the partial gas pressure inside the cavity and the degree of cavitation development.

Experimental Campaign #1~#5

Cavitation hysteresis

Figure 6 shows time histories of measured pressures, P_{tank}, P_{ch1}, P_{ch2} and P_{ch3} for the experimental campaign of #2-1st (U_{th}=7.9m/s, DO=20%). Qualitatively similar results were obtained for the other campaigns. In this typical case, the tank pressure P_{tank} is decreased from t=0s till 250s, and then it is increased from t= 250s. It is thought that when the curves of P_{tank} and P_{ch1} are in parallel, no cavitation occurs. On the curve of P_{tank}, inception and desinence of sheet cavitation detected by the naked eyes observation are indicated by the circles. Just after the inception, P_{ch1} is being constant, while P_{ch2} starts to decrease and the decrease rate is more than that of P_{tank}. Right after the measurement point of P_{ch2} is covered by the cavity, P_{ch2} becomes almost constant. With the further decrease of P_{tank}, P_{ch3} starts to decrease and then becomes constant due to the coverage by the sheet cavity. During the increase process of tank pressure, P_{ch3} and P_{ch2} rapidly increases in order, indicating that the measurement points become free from the cavity. After the sufficient increase of P_{tank}, the cavity finally diminishes. As shown, even in this low under-saturation level of the gas content, we observe the hysteresis between the inception and desinence.

Figure 7 shows an example of diagram of measured pressure (P_{ch1}, P_{ch2} and P_{ch3}) against tank pressure P_{tank}. The result of #2-1st (U_{th}=7.9m/s, DO=20%) is again used for the representation. To well illustrate the gas partial pressure inside the cavity, the measured pressures P_{ch} minus the vapor pressure P_v are plotted. The arrows indicate the direction of the process of given pressure change, i.e. the decrease/increase of P_{tank}. Thick part of the measured curves mean that the corresponding pressure tap is covered by the developed sheet cavity, and therefore assuming that the pressure inside the sheet cavity is a sum of the gas and vapor pressure, we can evaluate the gas partial pressure by $P_{ch} - P_v$. All curves

show the significant hysteresis between the decrease and increase processes of P_{tank}. From the thick part of Ch. 1 pressure, it can be found that P_{tank} at the desinence is larger than that at the inception. It is interesting to see that, at each measurement location of Ch. 1-3, the gas partial pressure slightly but apparently decreases just after the pressure tap is covered by the sheet cavity during the decrease process of P_{tank}. On the other hand, during the increasing process of P_{tank}, the gas partial pressure is almost constant although the sheet cavity continuously shrinks as can be recognized in the right-hand side photos. We do not know the physical mechanism of this phenomenon, but it might be that some amount of the gas inside the sheet cavity would be released in the form of gas bubbles from the trailing edge of the sheet cavity and the pressure of remained gas inside the sheet cavity would be kept constant.

Figure 8 shows the dimensionless measured pressures $\psi_{ch} = 2(P_{ch} - P_v)/\rho U_{th}^2$ against the cavitation number σ_{tank} for the experimental campaigns of #1~#3. The 1st data set are used for the representation. The curves with the different throat velocities U_{th} do not collapse into one, meaning that the flow similarity based on the cavitation number does not well hold despite that the gas content is small. Reynolds number was also different in these three cases; $\mathrm{Re} = 3.5\sim5.0 \times 10^4$, and therefore the combined effect of gas content and Reynolds number may appear in these cases.

Partial pressure of gas in sheet cavity

Figure 9 summarizes the gas partial pressure estimated by $P_g = P_{ch} - P_v$ in the experimental campaign of #1~#5. The gas pressure during the increase process of tank pressure has been employed since they are almost constant against the tank pressure. Figure

9(a) shows the influence of the throat velocity U_{th} on P_g under the low gas content level (#1~#3, DO=20%), while Fig. 9(b) shows the influence of the gas content DO under high throat velocity (#3~#5, $U_{th} \approx 9.0\mathrm{m/s}$). All three measurements (1st~3rd) are plotted together, showing that a fair repeatability of experiment can be confirmed despite the measured pressure is quite low. First of all, it is seen that the gas partial pressure P_g is clearly recognized with the order in hundred to thousand pascals. The order of this estimated gas partial pressure is similar to that obtained by Brennen [6] who measured the pressure inside super cavity behind a spherical headform. It is also seen that P_g at the nozzle throat (Ch. 1) is larger than those at Ch. 2 and Ch. 3, while at Ch. 2 and Ch. 3 P_g is almost the same. We suppose that, at the nozzle throat, the equilibrium condition has not yet been achieved and the pressure can be a little larger due to the rapid mass transfer of the dissolved gas to the cavity there. Or, we suspect that the measurement error due to the bubble accumulation in the pressure tube is in-negligible at this location. It is interesting to see from Fig. 9(a) that P_g at Ch. 2 and Ch. 3 are almost the same and they are almost constant in the low DO condition of around 20% regardless of the throat velocity U_{th}. We do not have any clear explanation for this in-sensitivity of gas partial pressure to the flow velocity. The turbulent diffusion of the dissolved gas may be more dominant than the convection in the determination of gas partial pressure inside the cavity; the turbulent Peclet number may be low. But, further investigation is necessary to understand the detailed mechanism determining the gas partial pressure. On the other hand, by increasing the gas content, i.e. DO from 20% to 60%, the gas partial pressure P_g is more likely to increase at all Ch. 1, Ch. 2 and Ch. 3 as shown in Fig. 9(b). However, the increment of P_g is not very large than one may expect from the high saturation level of dissolved oxygen.

Figure 10 summarizes the dimensionless gas partial pressure $\psi_g = 2P_g/\rho U_{th}^2$. Figure 10(a) shows the effect of the throat velocity U_{th} on ψ_g under the low gas content level (#1~#3, DO=20%), while Fig. 10(b) shows the effect of the gas content DO under high throat velocity (#3~#5, $U_{th} \approx 9.0\mathrm{m/s}$). All three measurements (1st~3rd) are plotted together, showing again that a fair repeatability of experiment can be confirmed. Looking at ψ_g at Ch. 2 and Ch. 3 in Fig. 10(a), it is seen that they decrease with the increase of the throat velocity U_{th}. This means that in the high velocity condition, the influence of gas content on the flow similitude using cavitation number would be negligible for very developed cavitation. ψ_g in #3 is about 0.02, and the difference of ψ_g between #1(U_{th} =6.3m/s) and #3(U_{th} =9.0m/s) is about 0.02. By increasing the gas content DO, the dimensionless gas pressure ψ_g increases and the order of increase is about 0.02 within the present DO conditions.

Experimental Campaign #6~#9

Cavitation characteristics: length and its fluctuation

Figure 11 shows the time-averaged cavity length normalized by the nozzle throat height, l_c/h, plotted against the cavitation number σ_{tank} for various DO conditions. The cavity lengths were obtained through the image analysis, which had been conducted for the experimental campaigns #6~#9 with the branch numbers of 1~3; short stable cavity, fluctuating sheet cavity with small amplitude, and fluctuating long sheet cavity with large amplitude were observed. The horizontal dashed curves indicate the location of pressure taps Ch. 1~ Ch. 4. It can be roughly found that the time-averaged cavity lengths are larger for the gas content of DO=70% and 50% than those for DO=30% and 10%, which indicates

that the mass diffusion of gas enhances the development of cavitation. Figure 12 shows (a) time histories of cavity lengths and (b) FFT spectra of cavity length fluctuation for the first data set of #6-1~#6-3 as examples. It can be confirmed that in #6-1 cavity length is short and almost stable, while in #6-2 and #6-3 sheet cavity fluctuates with high/low frequency and small/large amplitude. It is also found that, in the case of #6-1 and #6-2, the pressure taps of Ch. 1 and Ch. 2 are always covered by the cavity, while the pressure taps of Ch. 1~Ch. 3 in the case of #6-3 are almost always covered. In the case of #6-4, although the cavity length is not measured, a stable long sheet cavity is observed and covers all pressure taps of Ch. 1~Ch. 4. The partial pressure of gas inside the cavity can be estimated by those pressure taps covered by the cavity, which will be shown later. From Fig. 12(b), we can recognize a distinct frequency component of cavity length fluctuation especially for #6-2 and #6-3; the dominant frequency is 20.6 Hz and 9.1 Hz, respectively. In the case of #6-3, the peak frequency may locate near 40 Hz, but it is not very clear. Figure 13 summarizes the dominant frequency of cavity length fluctuation for all experimental campaigns of #6~#9 plotted against the cavitation number σ_{tank}. It is clear that the dominant frequency decreases with the decrease of cavitation number. As we mentioned before, clear periodical shedding of cloud cavity did not occur in the present experiment, probably due to the low Reynolds number of the flow as reported in Ref. [19]. Nevertheless, we still observe the cavity length fluctuation. The decrease tendency of the dominant frequency against the decrease of cavitation number is consistent with that of generally observed periodical cloud cavity shedding, but this tendency might be led by the decrease of the stiffness of the flow due to the increase of cavity volume.

Partial pressure of gas in sheet cavity

Figure 14 summarizes (a) measured pressure P_{ch} at Ch.1 ~Ch. 4 and (b) estimated partial pressure of gas in the cavity P_g plotted against the tank pressure P_{tank} in the experimental campaigns of #6~#9. In Fig. 14(a), it is clearly seen that the measured pressure P_{ch} converges toward the pressure measured at Ch. 1, P_{ch1}, as P_{tank} decreases. From this figure along with the high speed camera observation and the measurement of cavity length, the pressure inside the cavity can be specified. Then, the partial pressure of gas is estimated by $P_g = P_{ch} - P_v$ and is plotted in Fig. 14 (b). It is clearly found that P_g decreases with the decrease of P_{tank}. As Brennen [6] has mentioned, it is thought that the mass diffusion of dissolved gas into the sheet cavity occurs mainly near the leading edge of the cavity due to the large gradient of gas content with the small thickness of boundary layer of dissolved gas concentration. The diffusion itself seems to be not significantly influenced by the tank pressure P_{tank} since it is a local phenomenon. On the other hand, with the decrease of P_{tank}, the cavity volume significantly increases as it can be easily imagined from the cavity length shown in Fig. 11. Therefore, the gas density inside the cavity could be small for the lower tank pressure, resulting in the low partial pressure of gas inside the cavity; the gas partial pressure decreases with the development of cavitation.

Figure 15 shows the normalized gas pressure $\psi_g = 2P_g/\rho U_{th}^2$ against the cavitation number σ_{tank} in the experimental campaigns of #6~#9. Firstly, looking at the range with $\sigma_{tank} < 1.38$ where the significantly developed stable sheet cavity forms, the normalized gas pressure is $\psi_g = 0.01 \sim 0.03$. It is found that, with the increase of cavitation number σ_{tank}, ψ_g increases, and at the largest cavitation number in the present study ($\sigma_{tank} \approx 1.5$), ψ_g is roughly 0.03. This means that the deviation of the similarity of

cavitation using cavitation number is larger for the development stage of cavitation than for the significantly developed cavitation. Although this deviation is not very significant, it might be still in-negligible if the critical design of hydraulic machines is required even now and in the future.

CONCLUSIONS

In the present study, we successfully measured the cavity pressure and the gas partial pressure inside the sheet cavity at the throat of a converging-diverging nozzle. Two series of experimental campaigns #1~#5 and #6~#9 were conducted to understand the characteristics of partial pressure of gas inside the sheet cavity through the careful measurement of nozzle wall pressure using high precision pressure transducers.

In #1~#5, we focused on the hysteresis of cavity pressure and the influences of the flow velocity and the gas content (amount of dissolved oxygen) on the gas partial pressure inside the significantly developed sheet cavity. The hysteresis of cavity pressure as well as of the development of cavitation was clearly observed. It was also found that, even in low gas content level (about 20% of saturated DO condition under atmospheric pressure), the cavity pressure was slightly but apparently higher than the saturated vapor pressure, indicating the presence of gas partial pressure. It was also found that the gas pressure was almost constant regardless of the flow velocity but slightly increased against the increase of the saturation level of dissolved gas. Unfortunately, we are not able to give the clear explanations of the in-sensitivity of the partial gas pressure to the flow velocity and also of the weak sensitivity to the gas content. The detailed mechanism of mass transfer due to gas diffusion should be explored, which we would like to try in our future study.

In #6~#9, we focused on the cavity pressure inside sheet cavity under four development stages of cavitation; steady small sheet cavity, fluctuating sheet cavity with small amplitude, fluctuating long sheet cavity with large amplitude and significantly developed cavitation, which appear in the order with the decrease of cavitation number. Note that we did not observe the well-known periodical cloud cavity shedding associated with the re-entrant jet dynamics probably due to the low Reynolds number flow. It was observed that the partial pressure of gas in the cavity decreases, as the cavity is developed by decreasing the upstream tank pressure, or in other words decreasing the cavitation number.

On the law of similitude for cavitation using cavitation number, the possible deviation due to the presence of gas partial pressure in dimensionless form was the order of 0.01~0.03 in the present configuration and experimental conditions. Although this deviation is not very significant, it might be still in-negligible if the critical design of hydraulic machines is required even now and in the future.

ACKNOWLEDGMENT

We would like to thank to Dr. Yuichi Kunishima, a former postdoctoral researcher in Kyushu University, for his meaningful discussion from the view point of numerical modeling.

FUNDING

This work was partly supported by JSPS KAKENHI Grant Number JP20K04269.

NOMENCLATURE

B	Width of test section and nozzle throat
DO	Relative amount of dissolved oxygen [%] against saturation under standard condition
Fr	Froude number ($= U_{th}/\sqrt{gB}$)
f	Frequency of cavity length fluctuation
H	Height of test section
h	Height of nozzle throat
l_c	Cavity length
$P_{ch(i)}$	Measured pressure at i-th pressure tap ($i = 1,2,3,4$)
P_g	Partial pressure of gas inside cavity
P_{tank}	Pressure in upstream tank
P_v	Vapor pressure
P_w	Cavity outer wall pressure
Q	Volumetric flow rate
R	Curvature radius of cavity surface
Re	Reynolds number ($= U_{th}h/\nu$)
U_{th}	Nozzle throat velocity ($= Q/Bh$)
T	Surface tension

t	Time
We	Weber number
ρ	Density of water
σ	Cavitation number
σ_{tank}	Cavitation number defined by $2(P_{tank} - P_v)/\rho U_{th}^2$
$\psi_{ch(i)}$	Dimensionless pressure defined by $2(P_{ch(i)} - P_v)/\rho U_{th}^2$ $(i = 1,2,3,4)$
ψ_g	Dimensionless gas pressure defined by $2P_g/\rho U_{th}^2$

REFERENCES

[1] Brennen, C. E., 1995, *Cavitation and Bubble Dynamics*, Oxford University Press, Oxford, UK.

[2] ISO (International Organization for Standardization), 1987, *Centrifugal, mixed flow and axial pumps — Code for hydraulic performance tests — Precision grade*, ISO5198: 1987.

[3] Brennen, C. E., 1994, *Hydrodynamics of Pumps,* Concepts ETI, Vermont, USA, and Oxford University Press, Oxford, UK.

[4] Tsuru, W., Konishi, T., Watanabe, S. and Tsuda, S., 2017, "Observation of Inception of Sheet Cavitation from Free Nuclei," J. Therm. Sci., **26**(3), pp. 223-228. DOI : 10.1007/s11630-017-0933-8

[5] Amini, A., Reclari, M., Sano, T., Iino, M., Dreyer, M. and Farhat, M., 2019, "On the Physical Mechanism of Tip Vortex Cavitation Hysteresis," Exp. Fluids, **60**:118. DOI: 10.1007/s00348-019-2762-x

[6] Brennen, C. E., 1969, "The Dynamic Balances of Dissolved Air and Heat in Natural Cavity Flows," J. Fluid Mech., **37**(1), pp. 115–127. DOI: 10.1017/S0022112069000449

[7] Billet, M. L., and Weir, D. S., 1975, "The Effect of Gas Diffusion on the Flow Coefficient for a Ventilated Cavity," ASME J. Fluids Eng., **97**(4), pp. 501–505. DOI: 10.1115/1.3448090

[8] Parkin, B., and Ravindra, K., 1991, "Convective Gaseous Diffusion in Steady Axisymmetric Cavity Flows," ASME J. Fluids Eng., **113**(2), pp. 285–289. DOI: 10.1115/1.2909493

[9] Yu, P.-W., and Ceccio, S. L., 1997, "Diffusion Induced Bubble Populations Downstream of a Partial Cavity," ASME J. Fluids Eng., **119**(4), pp. 782–787. DOI: 10.1115/1.2819498

[10] Lee, I. H., Makiharju, S. A., Ganesh, H. and Ceccio, S. L., 2016, "Scaling of Gas Diffusion into Limited Partial Cavities," ASME J. Fluids Eng., **138**(5): 051301. DOI: 10.1115/1.4031850

[11] Iben, U., Wolf, F., Freudigmann, H. A., Frohlich, J. and Heller, W., 2015, "Optical Measurements of Gas Bubbles in Oil Behind a Cavitating Micro-Orifice Flow," Exp. Fluids **56**: 114. DOI: 10.1007/s00348-015-1979-6

[12] Kowalski, K., Pollak, S., Skoda, R., and Hussong, J., 2018, “Experimental Study on Cavitation-Induced Air Release in Orifice Flows,” ASME. J. Fluids Eng., **140**(6): 061201. DOI: 10.1115/1.4038730

[13] Zhou, J., Vacca, A., and Manhartsgruber, B., 2013, “A Novel Approach for the Prediction of Dynamic Features of Air Release and Absorption in Hydraulic Oils.” ASME. J. Fluids Eng., **135**(9): 091305. DOI: 10.1115/1.4024864

[14] Singhal, A. K., Athavale, M. M., Li, H., and Jiang, Y., 2002, “Mathematical Basis and Validation of the Full Cavitation Model,” ASME J. Fluids Eng., **124**(3), pp. 617–624. DOI: 10.1115/ 1.1486223

[15] Freudigmann, H., Dörr, A., Iben, U., and Pelz, P. F., 2017, “Modeling of Cavitation-Induced Air Release Phenomena in Micro-Orifice Flows,” ASME. J. Fluids Eng., **139**(11): 111301. DOI: 10.1115/1.4037048

[16] Gadd, G. E., and Grant, S., 1965, “Some Experiments on Cavities Behind Disks,” J. Fluid Mech., **23**(4), pp. 645–656. DOI: 10.1017/S002211206500160X

[17] Washio, S., 2015, *Recent Developments in Cavitation Mechanisms, A Guide for Scientists and Engineers*, Elsevier.

[18] Watanabe, S., Enomoto, K., Yamamoto, Y. and Hara, Y., 2014, “Thermal and Dissolved Gas Effects on Cavitation in a 2-D Convergent-Divergent Nozzle Flow,” Proc. the ASME 2014 4th Joint US-European Fluids Engineering Division Summer Meeting, Chicago, Illinois, **2**, FEDSM2014-21902, V002T06A013. DOI: 10.1115/FEDSM2014-21902

[19] Pelz, P., Keil, T. and Groß, T., 2017, “The Transition from Sheet to Cloud Cavitation,” J. Fluid Mech., **817**, pp. 439-454. DOI: 10.1017/jfm.2017.75

Figure Captions List

Fig. 1 Schematic view of test loop. White arrows indicate flow path of working fluid.

Fig. 2 Experimental apparatus of test nozzle with main dimensions including location of pressure taps. Estimated manufacture error is within 0.05mm.
(a) Dimensions of convergent divergent nozzle (in mm)
(b) Locations of pressure taps along nozzle wall (in mm)

Fig. 3 Examples of time histories of given pressure change of P_{tank} for experimental campaign of #1-1st (U_{th}=6.3m/s), #2-1st (7.9m/s) and #3-1st (9.0m/s)

Fig. 4 Examples of shadowgraph images of cavity for different DO and σ. Coverage of pressure taps Ch.1~Ch.4 by cavity can be recognized.
(a) DO=10%
(b) DO=30%
(c) DO=50%
(d) DO=70%

Fig. 5 Image analysis of cavity for determination of cavity length l_c through 3 steps.

Fig. 6 Example of time histories of measured pressure for experimental campaign of #2-1st (U_{th}=7.9m/s, DO=20%). Inception and desinence points of cavitation detected by naked eye observation are shown by circles.

Fig. 7 Example of estimated gas partial pressure P_{ch}-P_v plotted against tank pressure P_{tank} for experimental campaign of #2-1st (U_{th}=7.9m/s, DO=20%). Thickened part of each curve indicates that corresponding pressure taps are covered by cavitating region. Right-hand side photos show top and bottom views of cavitation at (1)-(3) during increasing process of P_{tank}.

Fig. 8 Examples of non-dimensional measured pressure ψ_{ch} – cavitation number σ_{tank} diagram for experimental campaign of #1-1st (U_{th}=6.3m/s), #2-1st (7.9m/s) and #3-1st (9.0m/s)

Fig. 9 Estimated partial pressure of non-condensable gas P_g plotted against nozzle throat velocity U_{th} (#1~3) and DO (#3~#5). Typical uncertainties with 95% confidence level for P_g and U_{th} are 0.20kPa (Ch.1 and 2), 0.012kPa (Ch.3) and 0.3m/s. DO varies before and after each test as shown in Table 1.
(a) Effect of flow velocity (#1~#3)
(b) Effect of DO (#3~#5)

Fig. 10 Non-dimensional gas partial pressure ψ_g plotted against nozzle throat velocity U_{th} (#1~#3) and DO (#3~#5). Typical uncertainties with 95% confidence level for ψ_g are 0.012 for Ch.1 and Ch.2 while 0.003 for Ch.3.
(a) Effect of flow velocity (#1~#3)
(b) Effect of DO (#3~#5)

Fig. 11 Time-averaged cavity length obtained from image analysis for different DO and σ_{tank}. Locations of pressure measurement taps are indicated by dashed lines. Estimated uncertainty with 95% confidence level is 0.07 for l_c/h and 0.10 for σ_{tank}.

Fig.12 Examples of time histories and FFT analyses of cavity length fluctuation for experimental campaign of #6-1st. Dashed lines in (a) indicate locations of pressure taps Ch.1~Ch.4. Distinct frequencies of cavity length fluctuation are clearly detected only in cases of #6-2 and # 6-3.
(a) Time history
(b) FFT analysis

Fig. 13 Frequency of cavity length fluctuation obtained by FFT analysis for different DO (#6~#9). Distinct frequency is detected only in each campaign with branch number of 2 and 3 shown in Table 3.

Fig. 14 Measured pressure and estimated gas partial pressure for different DO and σ_{tank}. Typical experimental uncertainties are 0.20kPa for Ch.1 and Ch.2, 0.05kPa for Ch.3 and 0.012kPa for Ch. 4, while that for tank pressure is 0.20kPa.
(a) Measured pressure
(b) Estimated gas partial pressure

Fig. 15 Gas pressure coefficient ψ_g plotted against cavitation number σ_{tank}. Typical uncertainties with 95% confidence level for ψ_g are 0.012 for Ch.1 and Ch.2 while 0.003 for Ch.3 and 0.002 for Ch.4.

Table Caption List

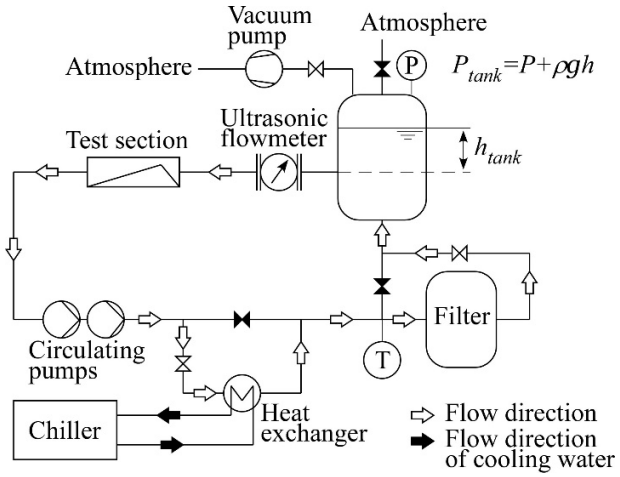

Fig. 1 Schematic view of test loop. White arrows indicate flow path of working fluid.

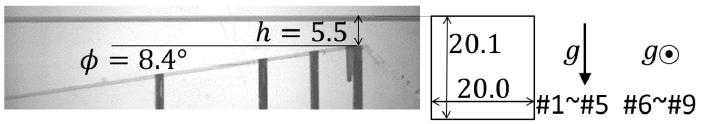

(a) Dimensions of convergent divergent nozzle (in mm)

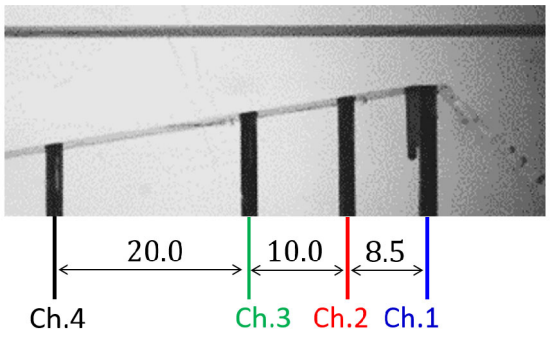

(b) Locations of pressure taps along nozzle wall (in mm)

Fig. 2 Experimental apparatus of test nozzle with main dimensions including location of pressure taps. Estimated manufacture error is within 0.05mm.

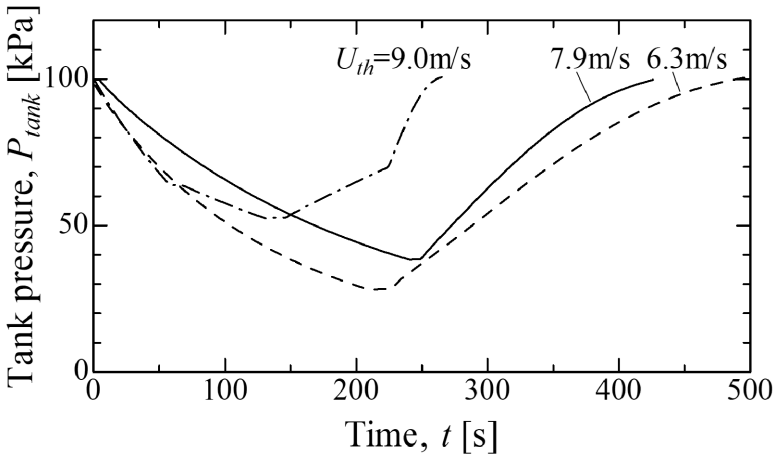

Fig. 3 Examples of time histories of given pressure change of P_{tank} for experimental campaign of #1-1st (U_{th}=6.3m/s), #2-1st (7.9m/s) and #3-1st (9.0m/s)

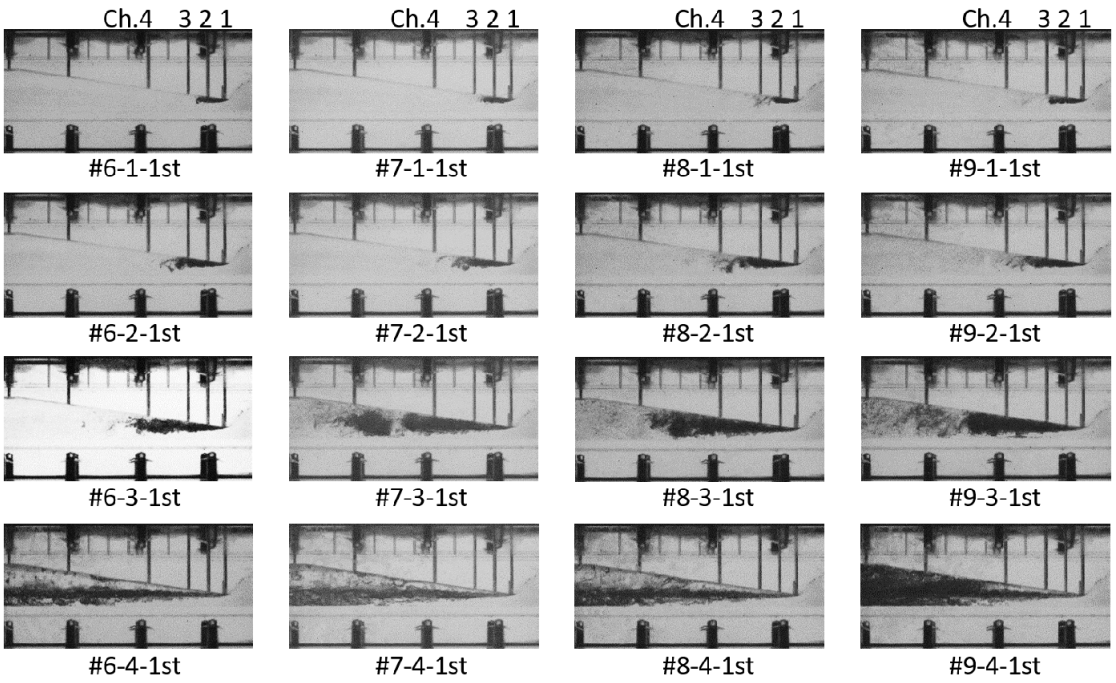

(a) DO=10% (b) DO=30% (c) DO=50% (d) DO=70%

Fig. 4 Examples of shadowgraph images of cavity for different DO and σ_{tank}. Coverage of pressure taps Ch.1~Ch.4 by cavity can be recognized.

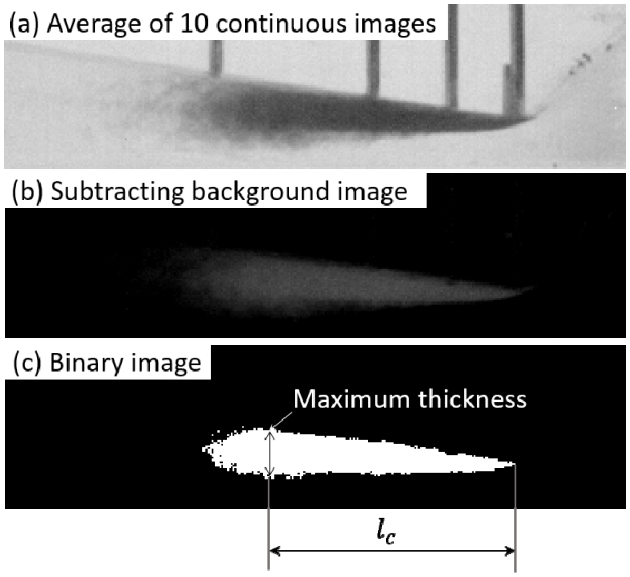

Fig. 5 Image analysis of cavity for determination of cavity length l_c through 3 steps.

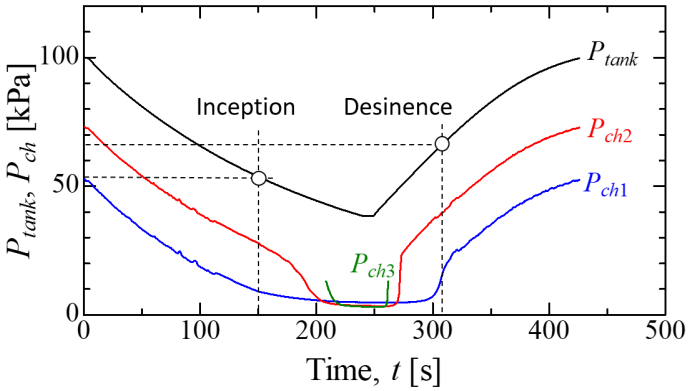

Fig. 6 Example of time histories of measured pressure for experimental campaign of #2-1st (U_{th}=7.9m/s, DO=20%). Inception and desinence points of cavitation detected by naked eye observation are shown by circles.

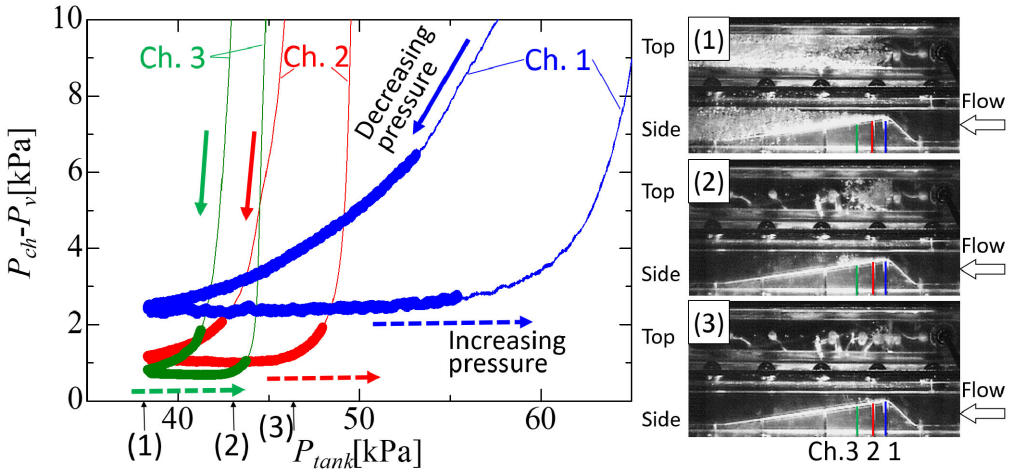

Fig. 7 Example of estimated gas partial pressure P_{ch}-P_v plotted against tank pressure P_{tank} for experimental campaign of #2-1st (U_{th}=7.9m/s, DO=20%). Thickened part of each curve indicates that corresponding pressure taps are covered by cavitating region. Right-hand side photos show top and side views of cavitation at (1)-(3) during increasing process of P_{tank}.

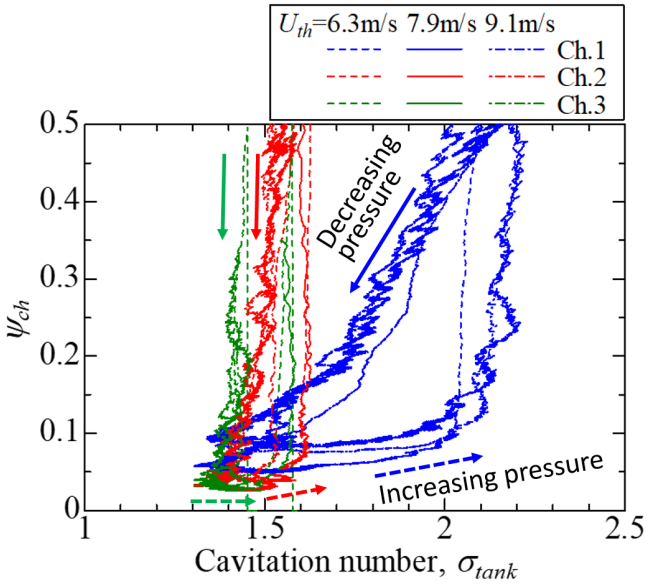

Fig. 8 Examples of non-dimensional measured pressure ψ_{ch} – cavitation number σ_{tank} diagram for experimental campaign of #1-1st (U_{th}=6.3m/s), #2-1st (7.9m/s) and #3-1st (9.0m/s)

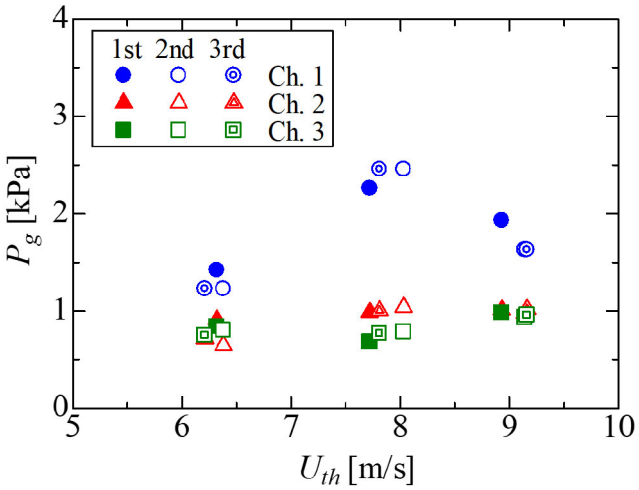

(a) Effect of flow velocity (#1~#3)

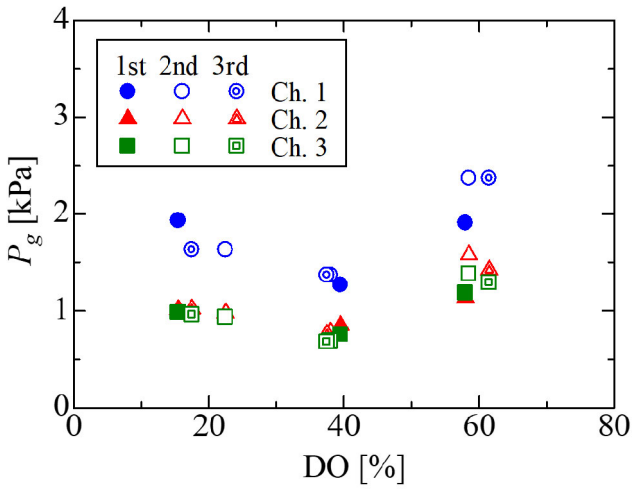

(b) Effect of DO (#3~#5)

Fig. 9 Estimated partial pressure of non-condensable gas P_g plotted against nozzle throat velocity U_{th} (#1~#3) and DO (#3~#5). Typical uncertainties with 95% confidence level for P_g and U_{th} are 0.20kPa(Ch.1 and 2), 0.013kPa(Ch.3) and 0.3m/s. DO varies before and after each test as shown in Table 1.

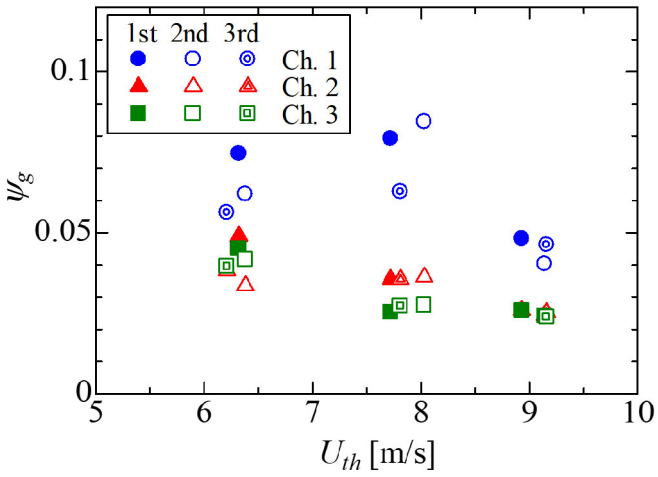

(a) Effect of flow velocity (#1-#3)

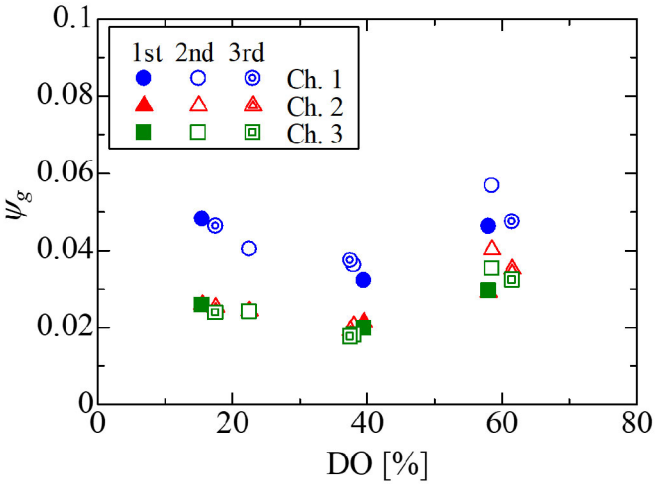

(b) Effect of DO (#3-#5)

Fig. 10 Non-dimensional gas partial pressure ψ_g plotted against nozzle throat velocity U_{th} (#1~#3) and DO (#3~#5). Typical uncertainties with 95% confidence level for ψ_g are 0.012 for Ch.1 and Ch.2 while 0.002 for Ch.3.

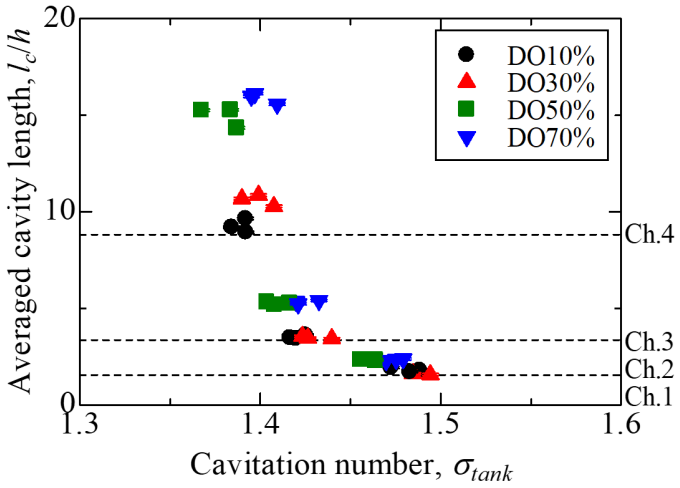

Fig. 11 Time-averaged cavity length obtained from image analysis for different DO and σ_{tank}. Locations of pressure measurement taps are indicated by dashed lines. Estimated uncertainty with 95% confidence level is 0.07 for l_c/h and 0.10 for σ_{tank}.

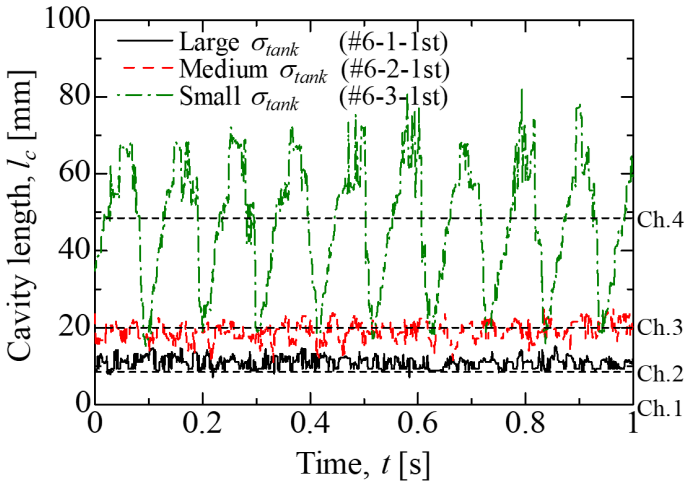

(a) Time history

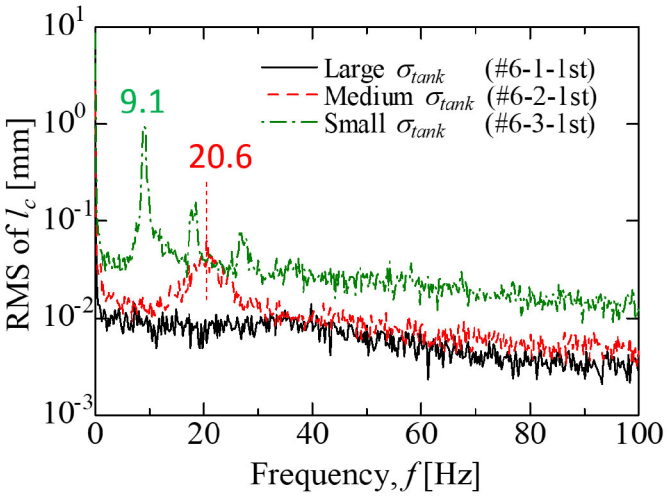

(b) FFT analysis

Fig. 12 Examples of time histories and FFT analyses of cavity length fluctuation for experimental campaign of #6-1st. Dashed lines in (a) indicate locations of pressure taps Ch.1~Ch.4. Distinct frequencies of cavity length fluctuation are clearly detected only in cases of #6-2 and # 6-3.

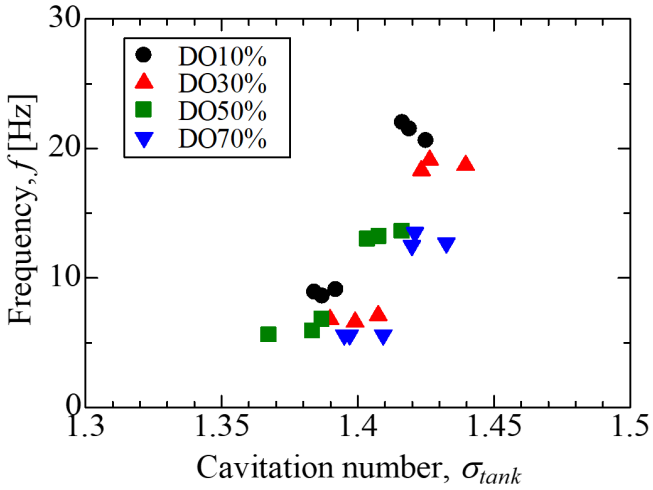

Fig. 13 Frequency of cavity length fluctuation obtained by FFT analysis for different DO (#6~#9). Distinct frequency is detected only in each campaign with branch number of 2 and 3 shown in Table 3.

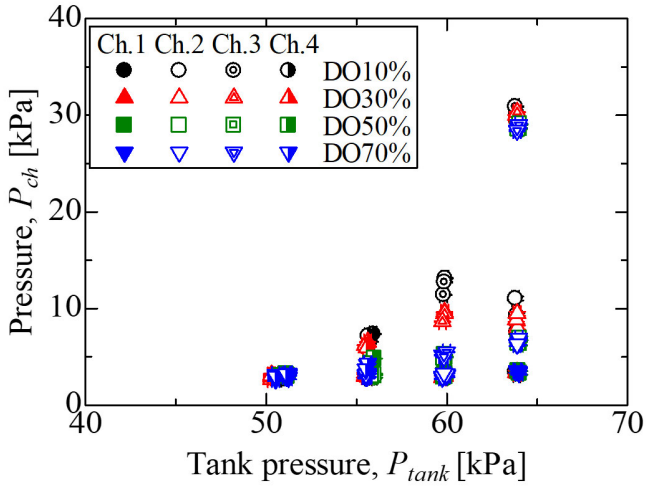

(a) Measured pressure

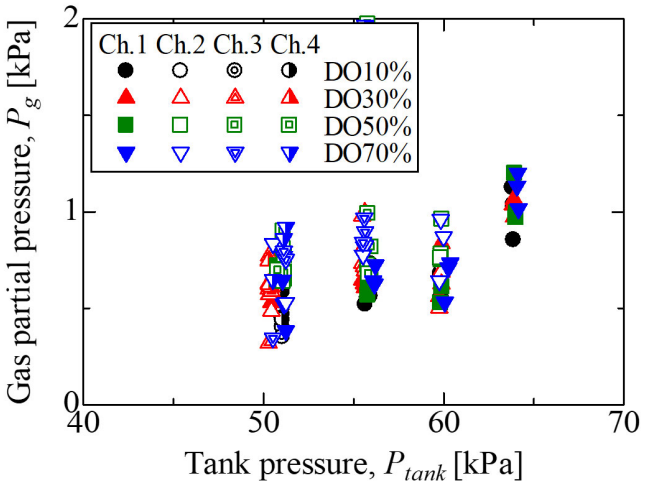

(b) Estimated gas partial pressure

Fig. 14 Measured pressure and estimated gas partial pressure for different DO and σ_{tank}. Typical experimental uncertainties are 0.20kPa for Ch.1 and Ch.2, 0.05kPa for Ch.3 and 0.012kPa for Ch.4, while that for tank pressure is 0.20kPa.

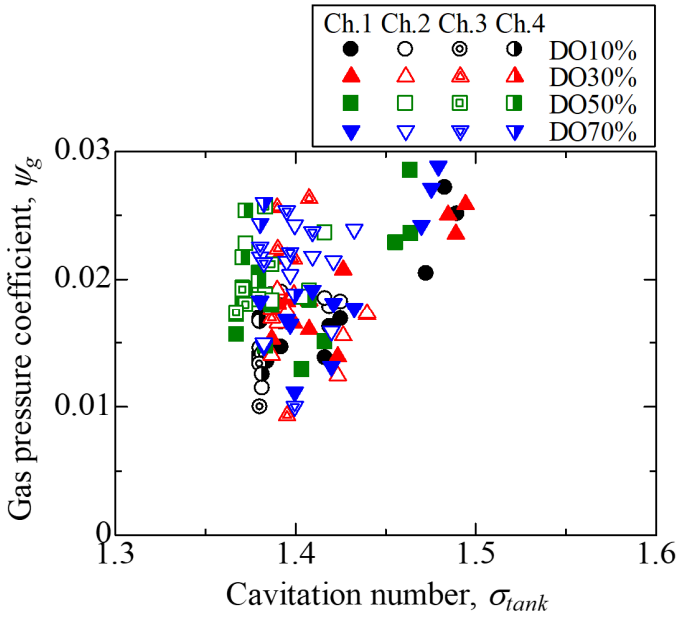

Fig. 15 Gas pressure coefficient ψ_g plotted against cavitation number σ_{tank}. Typical uncertainties with 95% confidence level for ψ_g are 0.012 for Ch.1 and Ch.2 while 0.003 for Ch.3 and 0.002 for Ch.4.

Table 1 Experimental conditions for experiment campaign #1~#5

No.	Velocity U_{th} [m/s]	Nominal DO [%]	Actual DO [%] (before and after) 1st	2nd	3rd
1	6.3 (6.2-6.4)	20	15 => 14	14 => 15	15 => 15
2	7.9 (7.7-8.0)	20	21 => 22	21 => 22	18 => 31
3	9.0 (8.9-9.1)	20	16 => 15	21 => 24	16 => 19
4	9.0 (8.9-9.1)	40	40 => 39	39 => 37	37 => 38
5	9.0 (8.9-9.1)	60	61 => 55	55 => 62	62 => 61

DO [%]: Amount of dissolved oxygen normalized by that at atmospheric pressure

Table 2 Pressure sensor arrangement for experiment campaign #1~#5

	Pressure sensors	Capacity	Accuracy
P_{tank}	GE sensing, UNIK5000 Grade: Improved accuracy	0-200kPa abs	0.1%RO (200Pa)
P_{ch1}		0-200kPa abs	0.1%RO (200Pa)
P_{ch2}		0-200kPa abs	0.1%RO (200Pa)
P_{ch3}		0-12kPa abs	0.1%RO (12Pa)
P_{ch4}		N.A.	N.A.

Table 3 Experimental conditions for experiment campaign #6~#9

No.	Velocity U_{th} [m/s]	Tank pressure P_{tank} [kPa]	Nominal DO [%]	Actual DO [%] (before and after) 1st	2nd	3rd
6-1	9.0 (8.9-9.1)	64	10 (10-20)	15 => 19	19 => 19	18 => 20
6-2		60		20 => 19	18 => 19	19 => 19
6-3		56		19 => 19	19 => 19	19 => 21
6-4		51		14 => 16	16 => 17	17 => 18
7-1		64	30	32 => 32	32 => 32	32 => 32
7-2		60		32 => 33	33 => 33	33 => 35
7-3		56		35 => 33	33 => 33	33 => 33
7-4		51		33 => 27	27 => 27	27 => 26
8-1		64	50	54 => 56	56 => 54	54 => 55
8-2		60		55 => 54	54 => 54	54 => 54
8-3		56		54 => 51	51 => 49	49 => 49
8-4		51		49 => 39	46 => 45	45 => 37
9-1		64	70	76 => 76	76 => 78	78 => 75
9-2		60		75 => 73	73 => 73	73 => 72
9-3		56		72 => 69	67 => 65	65 => 61
9-4		51		61 => 48	68 => 57	69 => 53

DO [%]: Amount of dissolved oxygen normalized by that at atmospheric pressure

Table 4 Pressure sensor arrangement for experiment campaign #6~#9

	Pressure sensors	Capacity	Accuracy
P_{tank}	GE sensing, UNIK5000 Grade: Improved accuracy	0-200kPa abs	0.1%RO (200Pa)
P_{ch1}		0-200kPa abs	0.1%RO (200Pa)
P_{ch2}		0-200kPa abs	0.1%RO (200Pa)
P_{ch3}		0-50kPa abs	0.1%RO (50Pa)
P_{ch4}		0-12kPa abs	0.1%RO (12Pa)